applied sciences

MDPI

Article

A Novel Method for Spectrometry Based on Imaging Systems

Rita Falconi [1,*,†], Stefania Sorbino [1,*,†], Roberto Pani [2,‡] and Luca Indovina [3,‡]

[1] Department of Medico-Surgical Sciences and Biotechnologies, Post-Graduate School in Medical Physics, Sapienza University of Rome, 00185 Rome, Italy
[2] Department of Medico-Surgical Sciences and Biotechnologies, Sapienza University of Rome, 00185 Rome, Italy; roberto.pani@uniroma1.it
[3] Department of Diagnostic Imaging, Oncological Radiotherapy and Hematology, Fondazione Policlinico Universitario Agostino Gemelli-IRCCS, Largo Agostino Gemelli 8, 00168 Rome, Italy; luca.indovina@policlinicogemelli.it
* Correspondence: rita.falconi@uniroma1.it (R.F.); stefania.sorbino@uniroma1.it (S.S.)
† These authors contributed equally to this work.
‡ Joint senior authorship.

Abstract: γ-ray spectrometry is a well-known technique in environmental radioactivity measurements where easily handled systems are needed. Scintillators coupled to a photomultiplier tube (PMT), are typically favoured over solid-state detectors as mobile spectrometers. Replacing PMT with position sensitive devices represents an innovative solution that provides the evaluation of the interaction point of the incident radiation. The knowledge of spectrometry as a function of the depth of interaction (DoI) assures a better understanding of the spectrum and a more reliable identification of the source. In this paper, the efficiency of a simple DoI estimator has been studied using a CRY018 monolithic crystal coupled to a multi-anode photomultiplier tube. The DoI estimator has been evaluated studying charge distributions and the dependency of spectrometric properties on the DoI has been qualitatively analyzed. The estimator has shown to be highly sensitive to the DoI, enabling a better understanding of the internal interaction processes of light and an efficient rejection of the background component on the spectra. The novelty of this work lies in the application of the DoI selection in spectrometry made available by the use of MAPMT. The proposed method is practical since it does not require complicated hardware solutions or complex computational procedures.

Keywords: environmental radioactivity measurements; DoI determination; γ spectrometry; imaging system; multiple sources identification

Citation: Falconi, R.; Sorbino, S.; Pani, R.; Indovina L. A Novel Method for Spectrometry Based on Imaging Systems. *Appl. Sci.* **2022**, *12*, 1657. https://doi.org/10.3390/app12031657

Academic Editor: Carlo Sabbarese

Received: 10 December 2021
Accepted: 18 January 2022
Published: 5 February 2022

1. Introduction

γ-ray spectrometry is a well-known technique in environmental radioactivity measurements. Modern application requirements need the use of brand-new detectors guaranteeing minimum weight and size, a high level of automation, multichannel and wireless connectivity. Nowadays, the most commonly used systems are easy to handle and to be carried by humans [1–3], assembled on air vehicles [4], robotic instruments [5], or dive into deep oceans aboard marine submersibles [6–8].

Facing this scenario, different types of detectors can be considered, such as scintillators (i.e., NaI:Tl) or solid-state detectors (i.e., HPGe), coupled to integrated electronic modules for data acquisition or custom-made designs to accommodate special needs. Scintillators are typically favored over solid-state detectors as mobile spectrometers since the latter traditionally require a cooling system with liquid nitrogen to operate, are generally more expensive, and are overall more sensitive in field deployment, despite the higher resolution they offer [9]. On the other hand, scintillators are sensitive to environmental conditions, especially temperature changes that may cause gain shifts during operation.

Since the invention of NaI:Tl by Hofstader in 1948, scintillators have been commonly coupled to a light-sensitive device such as the photomultiplier tube (PMT) [10]. Recent

advances in the development of semiconductor photodiodes have made silicon photomultiplier (SiPM) more suitable in some applications (i.e., when the position information is needed or in the presence of a magnetic field). These solid-state detectors are an array of many small-dimension avalanche photodiodes operated in Geiger mode. The high quantum efficiency (80–90% and therefore a better energy resolution), the low power consumption and the compact size have been promoting SiPM as the principal photodetector competitor of PMT. Furthermore, its peculiarity is to be intrinsically position sensitive (i.e., its structure is capable of localizing the position at which the centroid of light from a γ-ray event in the scintillator strikes the SiPM). To properly cover the entire sensitive area of the scintillator, a SiPM matrix is needed. The position information can be retained by using as many read out channels as the elements of the matrix. A further system with imaging capabilities but similar to PMTs is represented by a multi anode photomultiplier tube (MAPMT). Such systems could pave the way to finer light distribution analysis and to investigate γ spectrometric properties as a function of the depth of interaction (DoI).

In the field of environmental radioactivity measurements, a proper choice of the scintillation material ensures the best optimization of spectrometric performances in terms of detection efficiency, time response, and energy resolution. The widely employed scintillation crystal in γ spectrometry is NaI:Tl. It shows a high light yield (i.e., a good energy resolution) at a reasonable cost but its slow decay time prevents high count rate sources measurements. Moreover, its hygroscopic nature requires a bulky housing which limits the realisation of compact and handled systems.

The crystal showing the best properties in spectrometry applications is the $LaBr_3$:Ce. It has a strongly improved light yield and energy resolution and a fast response too, which is crucial in radioactivity measurements to spot high count rate sources. Moreover, its higher density guarantees a better detection efficiency and the possibility to realise smaller and compact detection systems. Nevertheless, this crystal is highly hygroscopic and it has a really expensive cost (i.e., about ten times higher than the NaI one) which limits its widespread use.

A solution accounting for the non-hygroscopic aspect while assuring a good trade-off among energy resolution, detection efficiency, and time response could be the use of the so-called CRY018 crystal. In the last five years, Crytur Company has released this new scintillator, made by mixed rare-earth silicate of unknown compounds [11]. Despite CRY018 showing a light yield similar to that of NaI:Tl, and a poorer energy resolution with respect to $LaBr_3$:Ce, it is comparable with the latter in terms of density (i.e., detection efficiency) and time response. Therefore CRY018 represents a good candidate for γ spectrometry showing halfway characteristics between the previous scintillation crystals.

In this work, the efficiency of a simple DoI estimator has been studied and verified using a round shape and white painted surfaces CRY018 monolithic crystal coupled to a MAPMT. The full reflective optical treatment enhances the spectrometric properties, as known in the literature [12,13] and affects the shape of the scintillation light distribution. In monolithic detectors, the DoI information is achieved by modelling the scintillation light distribution with analytical functions [14–16]. For this analysis a continuous DoI determination method previously proposed in [17–19] was chosen.

First, the DoI estimator has been evaluated studying charge distributions. Then, the dependency of spectrometric properties on the DoI has been investigated and qualitatively analyzed.

The proposed system allows to produce several spectra of the same sample (i.e., as a function of the DoI) offering the possibility to perform a better identification of the gamma emissions. In environmental radioactivity measurements, in fact, the background spectrum mainly due to the presence of the ^{238}U and ^{232}Th decay chain γ emissions, could be challenging to discriminate. The DoI discrimination of events allows reducing the background component, providing different ratios between a full energy peak and a Compton distribution as the selection goes deeper in the crystal. In general, the background affects the full energy peak counts, increasing the error on the activity evaluation of the source. As a consequence, the minimum detectable activity (MDA) would increase

worsening the detection efficiency. A further undesired background could be the presence of the self-absorption radiation emitted by the crystal itself. The imaging capabilities of the system could overcome this effect, enabling the use of crystals with self-activity. These scintillators have a greater Z_{eff} (effective atomic number) providing an improved detection efficiency. Hence, the knowledge of the spectrometry as a function of the DoI, enabled by choosing a position-sensitive device, could provide a better understanding of the spectrum and a more reliable identification of the source.

2. Materials and Methods

2.1. Experimental Set Up

Measurements were performed with a round shape (52 mm diameter and 6.25 mm thickness) CRY018 monolithic crystal. It was tested with an MAPMT equipped with an SBA (Super Bialkali) photocathode which guarantees a high quantum efficiency (up to 35%). All surfaces, except the one in contact with the photocathode, were polished and covered with white painting (0.2 mm of TiO_2). White painting is a typical feature for spectrometrical application increasing light collection [12,13].

The multi anode PMT used was a Hamamatsu H10966A-100 [20] with 64 independent anodes, made by a metal channel dynodes structure and a segmented anode pad of 8 × 8 array (6.08 mm pitch, 49 × 49 mm^2 active area). It reaches gains up to 3×10^5, a first dynode efficiency of 60% and an anodic gain variability of 1:2. Standard PMT collection efficiencies are usually higher, ranging from 80% up to 100%. This means that the best choice to have a system with imaging capabilities while maintaining similar or better performances in terms of efficiency and energy resolution requires the use of SiPM instead of MAPMT. A picture and a schematic top view of the MAPMT are shown in Figure 1.

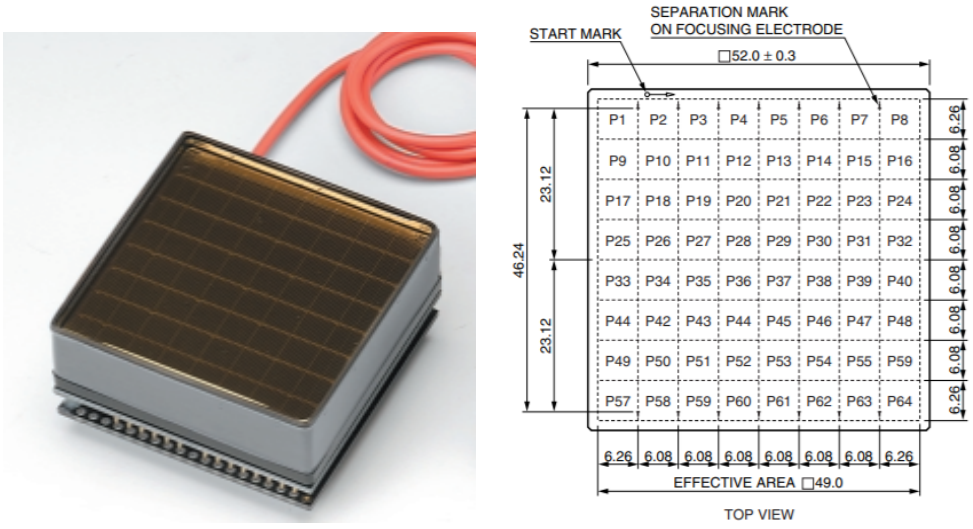

(**a**) (**b**)

Figure 1. Multi anode PMT Hamamatsu with its schematic top view [20]. (**a**) Multi anode PMT Hamamatsu H10966A-100. (**b**) Anode matrix view.

Four analog boards acquire in parallel the 64 anodic signal from the MAPMT, each channel being equipped with an operational amplifier in charge integration configuration (with an integrating capacitance of 22 pF and an input-output and supply range of ±10 V), a low injected charge (less than 1 pC) switch. After that a scintillation event has occurred in the crystal, constant voltages, proportional to the injected charge are present at the operational amplifier outputs. Two ADCs (analog to digital converter) with 14 bit resolution and eight parallel channels make the digital conversion. The hold signal is simultaneous on all of the 16 channels while the readouts are made sequentially and can be read on a parallel 14 bit bus common between two ADCs. The ADC sampling rate is programmable up to 250 Ksample/s, that is the maximum readout frequency of the system. The ADC

control and readout is performed by an FPGA board (field programmable gate array), that analyzes the data read in each time slot and discards those below a certain threshold. The FPGA firmware controls all the signals of the 4 analog PCBs and the download of the ADC collected data creating a suitable packet for the subsequent USB transmission. A picture and a schematic block of the whole system is shown in Figure 2.

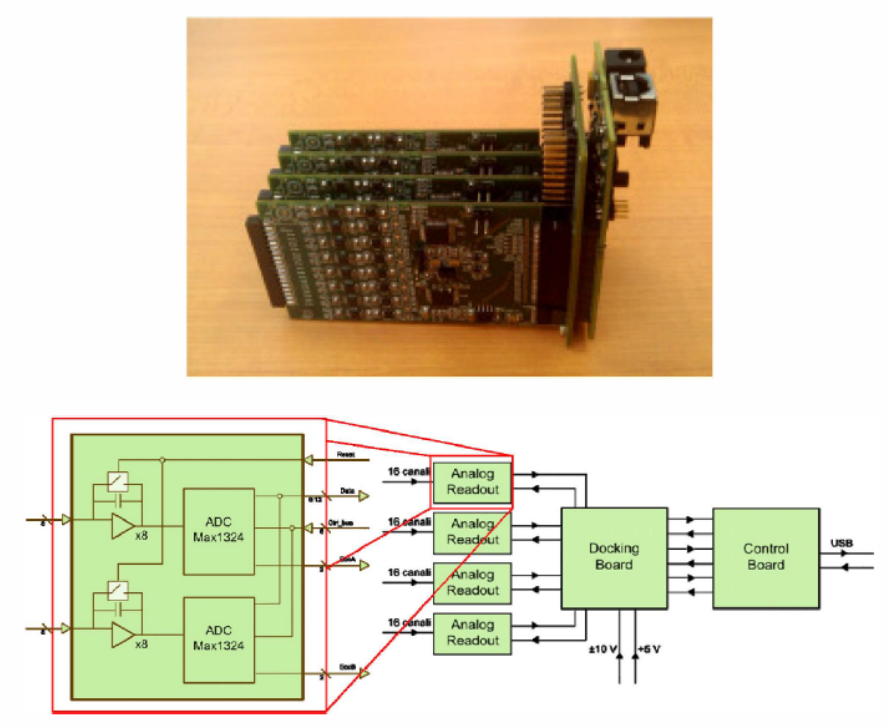

Figure 2. On the top part, a picture of the whole electronic system: four analog readout boards, a docking board and the FPGA based control board. On the bottom part, a block diagram representing the board configuration [21].

2.2. Methods

The CRY018 surface has been simultaneously irradiated by using 2.5 mm ^{57}Co and ^{133}Ba collimated sources in correspondence of an anode positioned near the center of the crystal surface. Both radionuclides are point sources absorbed in an ion-exchange bead approximately 1 mm in diameter. The bead is then fixed inside a solid plastic capsule 25 mm in diameter and 3 mm thick as shown in Figure 3. These sources are produced by "Eckert & Ziegler Nuclitec GmbH" and supplied with a proper certificate of calibration (BDR8152 and CTR8152, respectively, for ^{133}Ba and ^{57}Co product codes) and are characterized by the following activities: ^{133}Ba 2.51 MBq and ^{57}Co 1.96 MBq [22]. In Table 1, X-ray and γ emissions of the radioactive sources along with their branching ratio are reported.

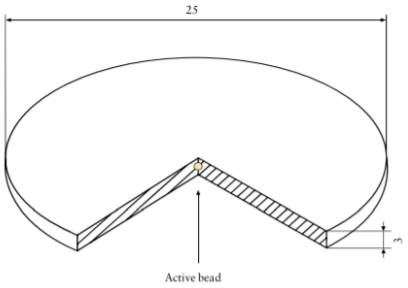

Figure 3. Schematic view of the radioactive housing [22].

Table 1. ^{133}Ba and ^{57}Co X-ray and γ emissions along with their branching ratio. In red energies corresponding to higher intensities are highlighted.

Radionuclide	Energy (keV)	BR (%)
^{133}Ba	30.6	33.9
	31.0	62.2
	35.0	20.7
	53.2	2.1
	79.6	2.7
	80.9	32.9
	160.6	0.6
	223.2	0.5
	276.4	7.2
	302.9	18.3
	356.0	62.1
	383.9	8.9
^{57}Co	14.4	9.2
	122.1	85.6
	136.5	10.7

The radioactive sources were directly arranged on the detector surface and housed inside a lead collimator (from the top, respectively, ^{133}Ba and ^{57}Co) of 1.25 mm radius and 39.45 mm length. The collimated geometry defines the most accurate solid angle resulting in a geometric efficiency of 2.5×10^{-4} and in this case, defines a count rate of about 630 counts/s and 490 counts/s, respectively, for ^{133}Ba and ^{57}Co sources, corresponding to a maximum dead time of 5%. A schematic view of the experimental and measurement setup is shown in Figure 4.

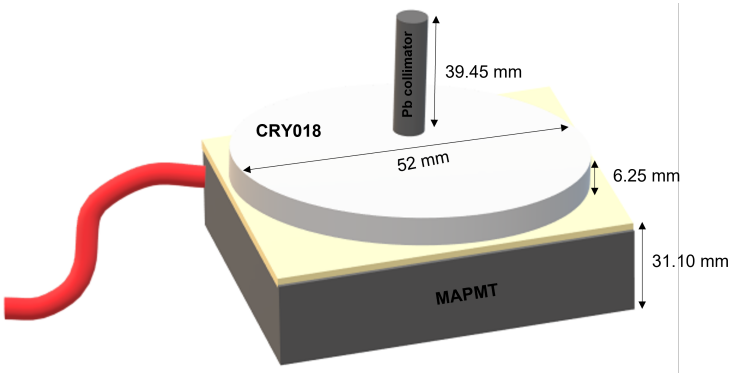

Figure 4. Schematic view of the experimental setup.

The double source irradiation allowed to investigate the DoI estimator parameter reliability as a function of the energy (γ emissions ranging from 31 keV to 356 keV). The choice of a monolithic scintillation crystal with a full reflective treatment assures a good spectrometry allowing the identification of the different full energy peaks generated by the source gamma emissions.

The DoI estimator parameter has been evaluated starting from the scintillation light distribution corresponding to each gamma emission energy. Thus, an energy selection on the spectrum is needed. Since the position-sensitive nature of the proposed system, the region of interest (ROI) method has to be taken into account and properly applied. In fact, the pulse height spectrum related to the spot irradiation shows the full energy peak but also a background component: the contribution of the photons that undergoes Compton scattering before reaching the detector, the diffuse contribution due to the lead collimator presence and the electronic noise. These additional factors impair peaks identification, introducing an error in the determination of the activity, which is related to the area below the peak. The ROI method allows to overcome this effect. It is possible to consider

just a selection on the image corresponding to the source in order to obtain a new pulse height spectrum in which the full energy peak is enhanced with respect to the background component. As a consequence, energy resolution performance can be improved.

First, the ROI method has been employed. Then, an energy selection on the new pulse height spectrum, based on an optimized window for each emission, has been applied to the events. For each event, the 64 MAPMT output signals are independently read out by 64 electronic channels and the sum of the collected charge is then related to the energy of the interaction itself. Hence, the charge distribution projection on one spatial axis for each gamma emission has been obtained too. These distributions have been produced averaging the charge collected from each anode over the total number of previously selected events and then projected along one axis. The DoI parameter has been estimated for each scintillation event. Four different depth regions have been identified based on this estimator. Finally, the validity of this parameter was verified by observing spectra as a function of the different depths of interaction.

2.3. Spectrometric Characteristics

A finer scanning on the CRY018 crystal surface has been previously carried out in [23,24] with the aim to characterize this scintillator in terms of energy resolution, pulse height uniformity response, and detection efficiency. A pulse height uniformity response within ±3% and an energy resolution less than 8.5% (∼30 keV) at 356 keV was reported. CRY018 has shown a fairly good energy resolution at 122 keV (12.7%, ∼15.5 keV) and at 81 keV (13.5%, ∼11 keV), too. In a 6 mm thick CRY018 a detection efficiency of ∼80% for 81 keV, 45% for 122 keV, and an efficiency less than 5% for energies greater than 356 keV was evaluated, too. This value could be further improved by increasing the thickness, considering standard dimensions for γ spectrometer that are of the order of few centimeters.

2.4. DoI Estimator Parameter

The DoI estimation method used in this work is based on the N/I parameter, previously proposed in [17]. This estimator is defined as the ratio of the integral of the scintillation light distribution (N) to its maximum (I).

The detected light distribution originated by each scintillation event in a monolithic crystal can be expressed through the Scrimger and Baker equation [25]:

$$f(x,y) = \frac{I}{\left(1 + \frac{x^2 + y^2}{t^2}\right)^{3/2}} \quad (1)$$

where I is the maximum of the distribution and t is the distance between the point of interaction and the photodetector (related to the DoI through the formula $DoI = T - t$, where T is the crystal thickness) and $r^2 = x^2 + y^2$ is the distance in the plane from the normal (a scheme is shown in Figure 5).

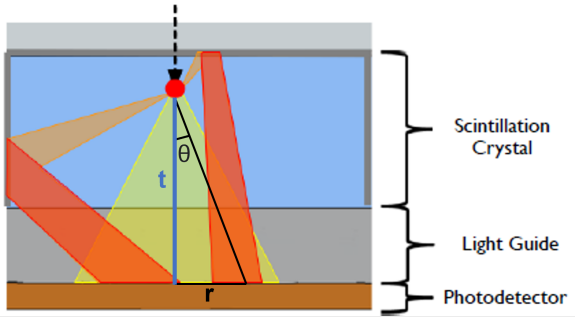

Figure 5. Scheme to illustrate the parameters in Scrimger and Baker formula.

It is possible to find the relation between N, I and the DoI by integrating Equation (1):

$$N = \int dx \int dy \frac{I}{\left(1 + \frac{x^2 + y^2}{t^2}\right)^{3/2}} \tag{2}$$

applying a conversion to polar coordinates it is possible to write the expression as follow,

$$N = \int d\theta \int dr \frac{I \cdot r}{\left(1 + \frac{r^2}{t^2}\right)^{3/2}} = 2\pi \left[\frac{I \cdot t^2}{\sqrt{(1 + \frac{r^2}{t^2})}} \right]_0^{+\infty} \tag{3}$$

Hence, the relation between N, I and the DoI parameters results in,

$$N = 2\pi \cdot I \cdot t^2 \Longrightarrow N/I \propto t^2 \tag{4}$$

The chosen electronic read out allows to know the charge value detected by each anode. These values fill up an 8×8 charge matrix, whose maximum represents I in the N/I ratio.

Starting from the obtained γ-ray spectra, an evaluation of the charge distributions and consequently of the N/I distribution for each visible energy peak was conducted. These distributions were divided into four different depth regions for each of which the resulting spectrum was obtained.

3. Results and Discussions

In Figure 6, the gamma-ray spectrum resulting from the irradiation of the 2.5 mm ^{57}Co and ^{133}Ba collimated sources is shown. The full energy peaks of the various emissions are well recognizable at 31, 81 and 356 keV for ^{133}Ba source and at 122 keV for ^{57}Co source. According to the characteristic data of ^{133}Ba radionuclide, the 31 keV line corresponds to an X-ray emission of the $K_{\alpha 1}$ line with nearly 62% emission intensity convoluted with the other two X-rays at 30.6 and 35 keV (see Table 1). The ability to detect low energies is an important issue in the questions related to the identification of radionuclides that are difficult to measure. 81 keV peak is the resulting convolution of the two emitted ^{133}Ba γs at 79.6 and 80.9 keV. The semi-logarithm scale enhances the high energies region allowing to identify 303 and 356 keV peaks. CRY018 energy resolution does not allow to discriminate the 136 keV peak from the 122 keV one as well as 276 keV from 303 keV.

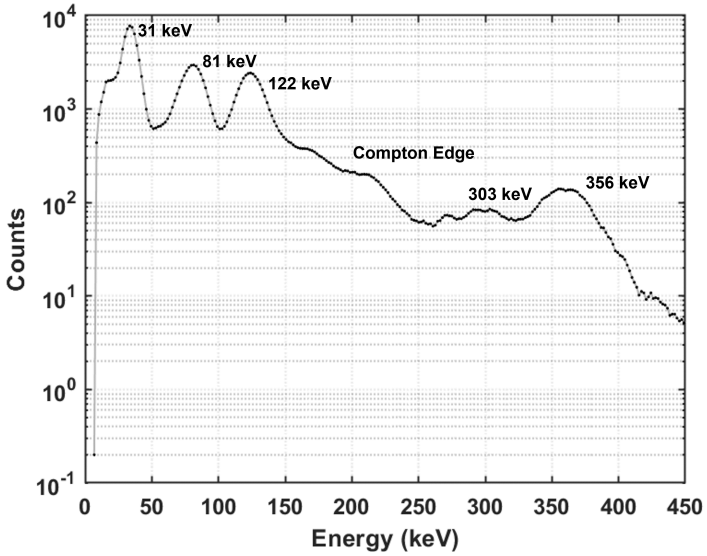

Figure 6. Gamma-ray spectrum resulting from the irradiation of the 2.5 mm ^{57}Co and ^{133}Ba collimated sources.

The pulse height spectrum resulting by the ROI selection on the image is shown in Figure 7.

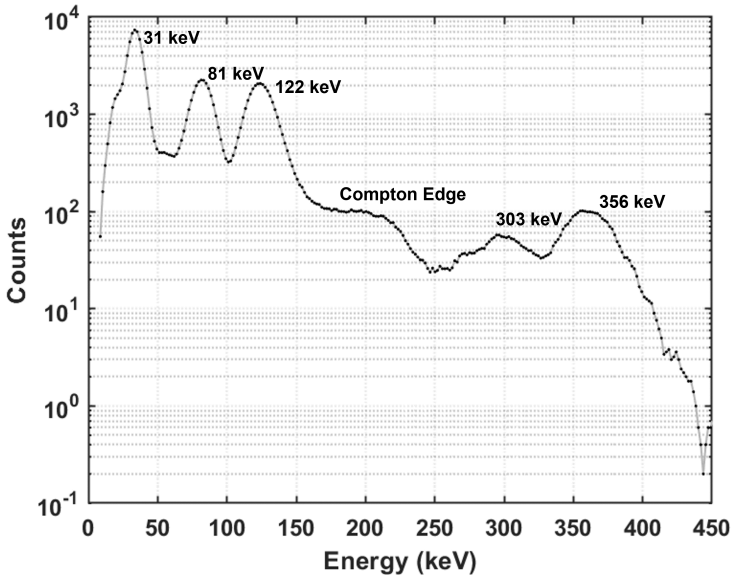

Figure 7. Gamma-ray spectrum resulting by the ROI selection.

It should be noted that the background has been clearly reduced using the ROI method (∼40%) allowing to better distinguish the lower intense 303 keV peak. The imaging capabilities assured by our system, allow to reject background events that can be produced for several reasons (i.e., Compton scattering and electronic noise below 20 keV). Moreover, it could also allow to simultaneously distinguish more radioactive sources located nearby the detector and to perform singular analysis just applying a selection on the events coming from each one of them. In Figure 8, the resulting averaged charge distribution projected along the *X* axis is shown. It can be observed how these distributions become more and more narrow and sharped as energy increases. This effect is due to the fact that inside a continuous crystal, emitted scintillation light spreads until the optical photons are detected on the photosensor. The extent of light dispersion depends on the distance between the light-emitting position (DoI position) and photosensor surface. Hence, high energy gamma emissions are expected to interact deeper inside the crystal (i.e., longer mean free paths) producing narrower light distributions with respect to lower energy gamma emissions.

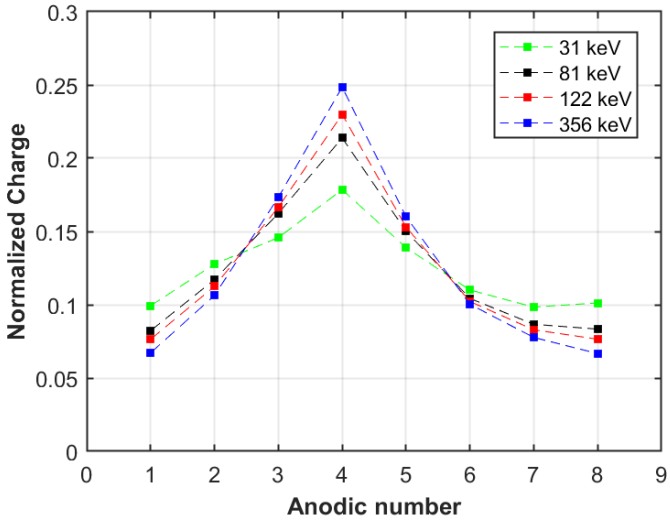

Figure 8. Projection on the *X* axis of the mean charge distributions for 31, 81, 122 and 356 keV corresponding to the irradiation of a central anode.

3.1. Analysis of the DoI-Dependent Light Collection

In Figure 9, the N/I distribution for each analyzed energy peak is shown. Only the higher intensity emissions in the spectrum have been taken into account for the DoI analysis (the ones highlighted in Table 1). The N/I parameter is small when the interaction event occurs at the bottom of the crystal (i.e., in the deepest region), whereas it increases if the scintillation event occurs at the top of the crystal (i.e., in the shallowest region).

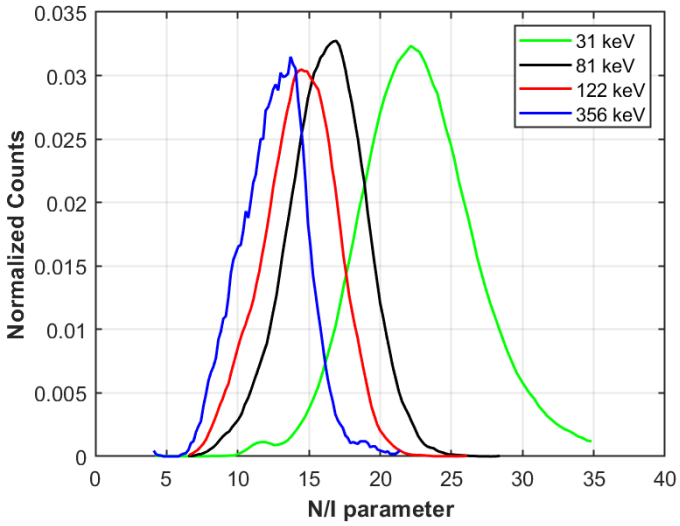

Figure 9. N/I parameter distributions for 31, 81, 122 and 356 keV.

It has to be noticed that the shape of the obtained distributions differs from the ideal case: they should be characterized by a rapid increase on the right side of the distribution (i.e., identifying the interactions occurring at the entrance of the crystal surface) and by a drop on the left side of the peak distribution following the attenuation law for gammas interacting deeper in the crystal. Experimentally, changes in N/I distribution are led by I fluctuations (i.e., the maximum of the collected charge by each event). Its variability is as high as the emission energy is low as it can be seen from Figure 9.

3.2. Spectrometry Proof of the N/I Parameter

The reliability of this parameter has been verified by dividing N/I distributions into four regions corresponding to a different layer of the crystal (i.e., depth) and by observing the resulting spectra for each region.

In Figure 10, the spectrum obtained for the first division is reported. The first region corresponds to the shallowest layer of the crystal (N/I parameter ranges from 25 to 35). In fact, as expected from the N/I distributions, only the 31 keV energy peak is clearly visible along with the background contribution given by the electronic noise (65% of the total number of events in the spectrum are related to 31 keV emission).

A finer selection starting from the upper limit of 31 keV N/I distribution (i.e., from 30 to 35), inside the first region, allows to investigate events that occurred in the surface proximity. As shown in Figure 11, this selection has strongly reduced source events enhancing the electronic noise component below 20 keV (25% for 31 keV vs. 75% for noise).

Hence, a proper selection in the range identified by the higher N/I parameters in the distribution allows to considerably reduce the electronic noise component in the pulse height spectrum. The capability offered by this parameter is crucial when low energy gamma emissions have to be properly measured.

In Figure 12, the spectra obtained for the following three division is reported.

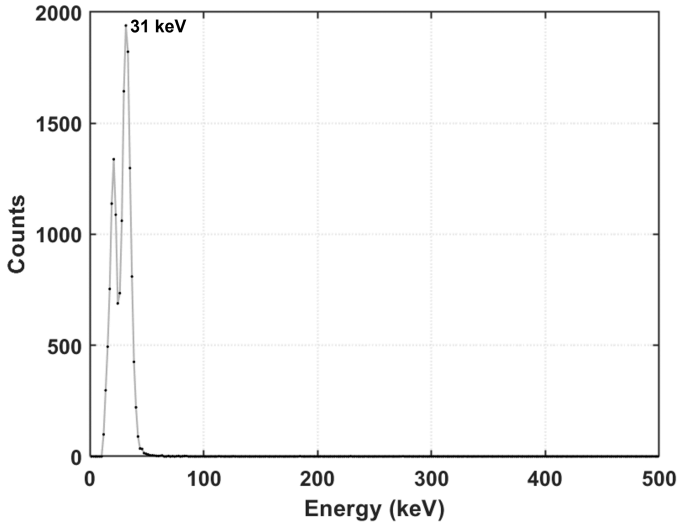

Figure 10. Spectrum resulting from the selection of events in the first depth region identified from the N/I parameter distributions (N/I from 25 to 35).

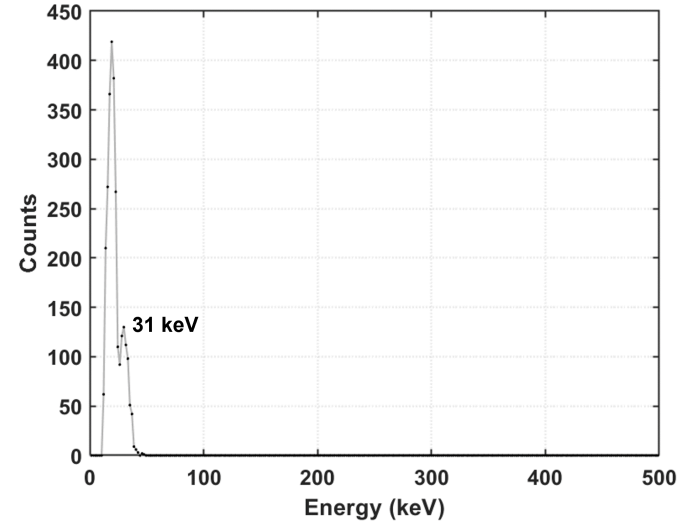

Figure 11. Spectrum resulting from a finer selection of events starting from the upper limit of the 31 keV N/I parameter distribution, contained in the first depth region (N/I form 30 to 35).

It is remarkable to notice how all the energy peaks visible in the spectra change in their shape as the next depth is selected. In Table 2, the mean free paths for the gamma emissions involved in this study are presented.

Table 2. Mean free path for gamma emissions in CRY018 spectrum.

Energy (keV)	λ (mm)
31	0.2
81	2.1
122	5.4
356	21

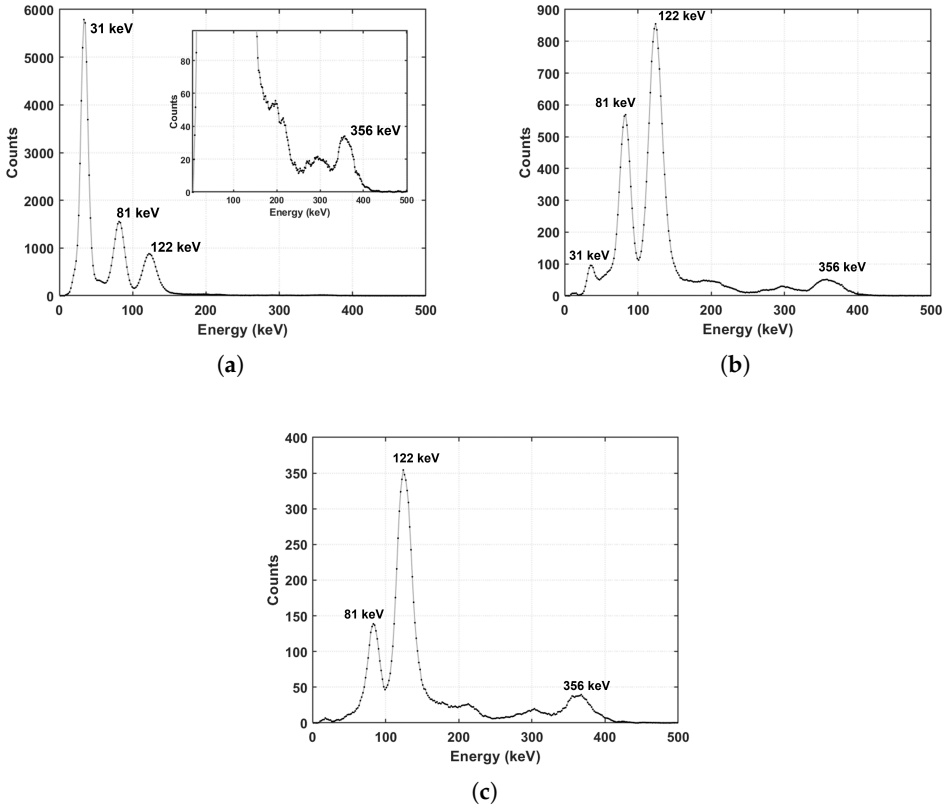

Figure 12. Gamma-ray spectra resulting for the next three depth regions identified from the N/I parameter distribution. (**a**) Spectrum resulting from the selection of events in the second depth region identified from the N/I parameter distributions (N/I from 15 to 25). A zoom on the 356 keV peak is reported, too. (**b**) Spectrum resulting from the selection of events in the third depth region identified from the N/I parameter distributions (N/I from 12 to 15). (**c**) Spectrum resulting from the selection of events in the fourth depth region identified from the N/I parameter distributions (N/I from 5 to 12).

The 31 keV gamma emission inside CRY018 has a mean free path of ≈0.2 mm and it is expected to interact in close proximity of the crystal surface. It is well-recognisable in the first spectrum, corresponding to the top layer (in this discussion the so called second depth region) of the crystal (Figure 12a), and it rapidly disappears as spectra at higher depths are observed (Figure 12b,c). The ratio of the 31 keV events for the three depth regions over those in the total spectrum resulted, respectively, in 72%, 1%, <1%. The 81 keV gamma emission interacts more likely at ≈2.1 mm but it is expected to be present along the entire thickness of the crystal (respectively for the three regions 67%, 26%, 7%). Similar considerations apply to 122 keV, whose mean free path is around 5.4 mm (respectively for the three regions 41%, 40%, 19%). Despite this, the high sensitivity of the N/I parameter allows to observe the differences in energy peaks formation due to their different interaction probability inside the crystal. In fact, the highest contribution to the 81 keV peak occurs in the second depth region (Figure 12a), corresponding to an intermediate crystal thickness, and gradually drops in the next depth regions whereas 122 keV peak still greatly contributes (Figure 12b,c). The 356 keV mean free path is considerably longer than the crystal size and its interaction probability inside the entire thickness is expected to be small and nearly constant. In Figure 12a, a zoom around 356 keV gamma emission is shown for a better visualisation. 356 keV peak integral for the three depth regions resulted, respectively, in 875, 893 and 879 counts (∼33% for each one) proving a close agreement with the expected interaction probability (i.e., following the attenuation law).

By simple qualitative observations based on the obtained spectra, the N/I parameter appears to be strictly related to the depth of interaction of events occurring inside the crystal and offers the possibility to conduct deeper analysis on spectrometry leading to more reliable identification of gamma emissions revealed by the detector.

4. Conclusions

In this work, a DoI parameter estimator has been evaluated using a 6 mm thick white painted CRY018 monolithic crystal coupled with a MAPMT. The scintillation material and the optical treatment were chosen to optimize MAPMT spectrometric performances in terms of collection of light, energy resolution, and pulse height uniformity response. Relying on simple spectrometric assessments, the DoI parameter has shown to be highly sensitive to the depth of interaction of photons, allowing to deeply understand the internal interaction processes of light. Moreover, the estimator allows to perform a DoI dependent events selection providing several spectra of the same sample which could be useful in multigamma emission sources measurements. Furthermore, the imaging capabilities of the proposed system offer new possibilities in γ-peaks investigation such as the use of an ROI method to better reject background events that affect countings and peak identification. Hence, the matching of the DoI with ROI enables new methods for an optimized identification of gamma peaks and finally of the revealed unknown radioactive source.

The novelty of this work lies in the application of the DoI selection in spectrometry enabled by the use of a position-sensitive system. The proposed method is particularly practical since it is simple to implement and does not require complicated hardware solutions or complex computational procedures. Finally, the investigation of new detectors such as the one proposed is important for the characterization of materials, whether they are environmental matrices or nuclear materials. In addition, the development of devices sensitive to low energies will become an important issue in the future, especially for questions related to radionuclides that are difficult to measure. Further analysis should be carried on using a larger crystal (i.e., size of the order of several cm, for practical applications) coupled to a SiPM device, in order to extend the analysis in a wider energy range and provide a proper calibration of N/I parameter with the crystal thickness.

Author Contributions: R.F. and S.S. have contributed for conceptualization, methodology, software, formal analysis, validation, data curation, visualization, writing—original draft preparation and writing—review and editing. Supervision, R.P. and L.I.; project administration, R.P. All authors have read and agreed to the published version of the manuscript.

Funding: This research received no external funding.

Conflicts of Interest: The authors declare no conflict of interest.

Abbreviations

The following abbreviations are used in this manuscript:

PMT	Photomultiplier Tube
MAPMT	Multi Anode Photomultiplier Tube
SiPM	Silicon Photomultiplier
ADC	Analog to Digital Converter
FPGA	Field Programmable Gate Array
DoI	Depth of Interaction
SBA	SuperBialkali
ROI	Region of Interest
ER	Energy Resolution

References

1. Kock, P.; Samuelsson, C. Comparison of airborne and terrestrial gamma spectrometry measurements—Evaluation of three areas in southern Sweden. *J. Environ. Radioact.* **2011**, *102*, 605–613. [CrossRef] [PubMed]
2. Cresswell, A.J.; Sanderson, D.C.W.; Harrold, M.; Kirley, B.; Mitchell, C.; Weir, A. Demonstration of lightweight gamma spectrometry systems in urban environments. *J. Environ. Radioact.* **2013** *124*, 22–28. [CrossRef]
3. Cresswell, A.J.; Sanderson, D.C.W.; Yamaguchi, K. Assessment of the calibration of gamma spectrometry systems in forest environments. *J. Environ. Radioact.* **2018**, *181*, 70–76. [CrossRef] [PubMed]
4. Simon, S.L.; Graham, J.C. A comparison of aerial and ground level measurements of ^{137}Cs in the Marshall Islands. *Environ. Monit. Assess.* **1998**, *53*, 363–377. [CrossRef]
5. Zalud, L.; Jilek, T.; Kocmanova, P. Robotic Autonomous Field Gamma Radiation Measurement for Environmental Protection. *Recent Advances on Energy and Environment*. Available online: http://www.wseas.us/e-library/conferences/2015/Budapest/EE/EE-09.pdf (accessed on 10 November 2021).
6. Hattori, M.; Okano, M. New Results of Sea Bottom Radioactivity Measurement. *JAMSTEC J. Deep Sea Res.* **2001**, *18*, 1–13. Available online: https://ci.nii.ac.jp/naid/10020374222/en/ (accessed on 10 November 2021).
7. Tsabaris, C.; Patiris, D.; Lykousis, V. KATERINA: An in situ spectrometer for continuous monitoring of radon daughters in aquatic environment. *Nucl. Instruments Methods Phys. Res. Sect. A* **2011**, *626–627*, S142–S144. [CrossRef]
8. Androulakaki, E.; Tsabaris, C.; Eleftheriou, G.; Kokkoris, M.; Patiris, D.; Pappa, F.; Vlastou, R. Efficiency calibration for in situ γ–ray measurements on the seabed using Monte Carlo simulations: Application in two different marine environments. *J. Environ. Radioact.* **2016**, *164*, 47–59. [CrossRef] [PubMed]
9. Clouvas, A.; Xanthos, S.; Antonopoulos-Domis, M. Radiological maps of outdoor and indoor gamma dose rates in Greek urban areas obtained by in situ gamma spectrometry. *Radiat. Prot. Dosim.* **2004**, *112*, 267–275. [CrossRef] [PubMed]
10. Bisogni, M.G.; Del Guerra, A.; Belcari, N. Medical applications of silicon photomultipliers. *Nucl. Inst. Methods Phys. Res. A* **2019**, *926*, 118–128. [CrossRef]
11. Crytur. Available online: https://www.crytur.com/materials/cry-18/ (accessed on 10 September 2020).
12. Pani, R.; Fabbri, A.; Cinti, M.N.; Orlandi, C.; Pellegrini, R.; Scafè, R.; Artibani, M. LaBr3:Ce small FOV gamma camera with excellent energy resolution for multi-isotope imaging. *J. Instrum.* **2015**, *10*, C06002. [CrossRef]
13. Lo Meo, S.; Baldazzi, G.; Bennati, P.; Bollini, D.; Orsolini Cencelli, V.; Cinti, M.N.; Lanconelli, N.; Moschini, G.; Navarria, F.L.; Pani, R.; et al. GEANT4 simulation for modelling the optics of LaBr scintillation imagers. *IEEE Trans. Nucl. Sci.* **2008**, 4964–4968. [CrossRef]
14. Lerche, C.W.; Ros, A.; Gadea, R.; Colom, R.J.; Toledo, F.J.; Herrero, V.; Monzo, J.M.; Sebastia, A.; Abellan, D.; Sanchez, F.; et al. DOI measurement with monolithic scintillation crystals: A primary performance evaluation. *IEEE Trans. Nucl. Sci.* **2007**, *4*, 2594–2600. [CrossRef]
15. Lerche, C.W.; Ros, A.; Herrero, V.; Esteve, R.; Monzo, J.M.; Sebastia, A.; Sanchez, F.; Munar, A.; Benlloch, J.M. Dependency of Energy-, Position- and Depth of Interaction Resolution on Scintillation Crystal Coating and Geometry. *IEEE Trans. Nucl. Sci.* **2008**, *3*, 1344–1351. [CrossRef]
16. Fabbri, A.; Bennati, P.; Orsolini Cencelli, V.; Cinti, M.; Pellegrini, R.; Petullà, F.; Pani, R.; Notaristefani, F. A new iterative algorithm for pixilated and continuous scintillating crystal distributious. *Nucl. Instrum. Methods Phys. Res. Sect. A Accel. Spectrometers Detect. Assoc. Equip.* **2011**, *648*, S79–S84. [CrossRef]
17. Pani, R.; Nourbakhsh, S.; Pani, P.; Bennati, P.; Lo Meo, S.; Cinti, M.N.; Pellegrini, R.; Cassano, B.; Bettiol, M.; Scafè, R. Continuous DoI determination by gaussian modelling of linear and non-linear scintillation light distributious. In Proceedings of the 2011 IEEE Nuclear Science Symposium Conference Record, Valencia, Spain, 23–29 October 2011; pp. 3386–3389. [CrossRef]
18. Pani, R.; Gonzalez, A.J.; Bettiol, M.; Fabbri, A.; Cinti, M.N.; Preziosi, E.; Borrazzo, C.; Conde, P.; Pellegrini, R.; Di Castro, E.; et al. Preliminary evaluation of a monolithic detector module for integrated PET/MRI scanner with high spatial resolution. *J. Instrum.* **2015**, *10*, C06006. [CrossRef]
19. Pani, R.; Bettiol, M.; Preziosi, E.; Borrazzo, C.; Pellegrini, R.; Gonzalez, M.A.; Conde, P.; Cinti, M.; Fabbri, A.; Di castro, E.; et al. A Novel Method for γ-photons Depth-of-Interaction Detection in Monolithic Scintillation Crystals. *IEEE Trans. Nucl. Sci.* **2016**, *63*, 2487–2495. [CrossRef]
20. HAMAMATSU. Available online: https://www.hamamatsu.com/eu/en/index.html (accessed on 10 September 2020).
21. Fabbri, A.; Galasso, M.; Cencelli, V.; Colace, L. Compact multi channel readout electronic for position sensitive photomultiplier tube. In Proceedings of the 2014 Fotonica AEIT Italian Conference on Photonics Technologies, Naples, Italy, 12–14 May 2014; pp. 1–3. [CrossRef]
22. Eckert & Ziegler Nuclitec GmbH. Available online: https://sales.isotopeproducts.com/ (accessed on 10 October 2020).
23. Pani, R.; Colarieti-Tosti, M.; Cinti, M.N.; Polito, C.; Trigila, C.; Ridolfi, S. Investigation of radiation detection properties of CRY-018 and CRY-019 scintillators for medical imaging. *J. Instrum.* **2016**, *11*, P09010. [CrossRef]

24. Pellegrini, R.; Camera, F.; Polito, C.; Falconi, R.; Bettiol, M.; Longo, M.; De Vincentis, G.; Indovina, L.; Pani, R.; Frantellizzi, V. Imaging performance dependence on crystal absorption properties: The CRY018 and CRY019 comparison. *J. Instrum.* **2020**, *15*, C05076. [CrossRef]
25. Scrimger, J.W.; Baker, R.G. Investigation of light distribution from scintillations in a gamma camera crystal. *Phys. Med. Biol.* **1967**, *12*, 101–103. [CrossRef] [PubMed]